Chemical Geology 275 (2010) 127–138

Contents lists available at ScienceDirect

Chemical Geology

journal homepage: www.elsevier.com/locate/chemgeo

Sources of methane inferred from pore-water $\delta^{13}C$ of dissolved inorganic carbon in Pockmark G11, offshore Mid-Norway

Yifeng Chen [a,b,*], William Ussler III [c], Haflidi Haflidason [d], Aivo Lepland [b], Leif Rise [b], Martin Hovland [e], Berit O. Hjelstuen [d]

[a] Key Laboratory of Marginal Sea Geology, Guangzhou Institute of Geochemistry, Chinese Academy of Sciences, PR China
[b] Geological Survey of Norway, Leiv Eirikssons vei 39, NO-7491 Trondheim, Norway
[c] Monterey Bay Aquarium Research Institute, 7700 Sandholdt Road Moss Landing, CA 95039, USA
[d] Dept. of Earth Science, University of Bergen, Allegt. 41, N-5007 Bergen, Norway
[e] Statoil ASA, 4035 Stavanger, Norway

ARTICLE INFO

Article history:
Received 1 December 2009
Received in revised form 22 April 2010
Accepted 23 April 2010

Editor: D.B. Dingwell

Keywords:
$\delta^{13}C_{DIC}$ of pore-water
Microbial methane
Recycling of fossil methane hydrate
Episodic methane fluxes
Pockmark G11
Vøring Plateau

ABSTRACT

Pockmark G11 is the most spectacular one among the pockmarks located at the southern border of Vøring Plateau and 1–2 km away from the northern flank of the Storegga Slide, mid-Norwegian continental margin. For the first time, detailed pore-water geochemical studies were conducted to address methane hydrate occurrence, methane seepage and associated geochemical processes, and methane characteristics in the pockmark. Pore-waters collected from five sediments cores inside and one sediment core outside the pockmark, were analyzed for dissolved Cl^-, sulfate (SO_4^{2-}), total hydrogen sulfide (ΣH_2S), Ca^{2+}, Mg^{2+}, dissolved inorganic carbon (DIC), $\delta^{13}C_{DIC}$ and $\delta^{18}O$. Methane hydrates were recovered in all sediments below 0.75 m in a core inside pockmark G11, which is in good accordance with heavy oxygen isotope (1.9 to 2.3‰SMOW) and low Cl^-concentrations (84.9 to 16.1 mM) in pore-waters. Pore-water profiles indicate that upward-migrating methane fluids are spatially variable in the pockmark, with methane fluxes ranging from below detection in the center and outside, to 0.30–0.54 mol m^{-2} a^{-1} inside. In the cores with active methane fluxes, maximum DIC concentrations (19.4 to 21.5 mM) and corresponding minimum $\delta^{13}C_{DIC}$ values (−52.3 to −54.6 ‰ PDB) occur within sulfate-methane-transition (SMT) zones from ~0.40 to 0.50 m below seafloor (mbsf), close to the seafloor. Simple mass balance modeling and $\delta^{13}C_{DIC}$ measurements within the SMT zones suggest that methane in shallow sediments within pockmark G11 is microbial in origin. Pore-water geochemistry and seabed observations suggest that methane fluxes inside pockmark G11 are episodic, and derived mostly from the recycling of methane hydrate at depth during sediment burial.

1. Introduction

Submarine pockmarks are widespread features on continental margins, often related to seepage of methane-rich fluids at the seafloor and/or to the presence of gas hydrate in the subsurface (e.g. Hovland and Judd, 1988). Pockmarks have received increased attention because they represent potential pathways for large quantities of methane and other fluids escaping from subsurface sediments to the ocean and, perhaps to the atmosphere (e.g. Paull et al., 2002; Ussler et al., 2003; Hovland et al., 2005; Gay, 2006). Since methane is a strong greenhouse gas, the global climate of the geological past might have been affected by the rapid release of large amount of methane from subsurface marine sediments (e.g., Kvenovlden, 1993; Dickens, 1999).

In active seepage sites, the upward migration of methane dominates the pore-water chemistry of near-surface sediment horizons. The anaerobic oxidation of methane (AOM) ascending toward the seafloor mediated by downward diffusion of sulfate from overlying seawater occurs within the sulfate-methane-transition (SMT) zone near the sediment surface, according to the net reaction $CH_4 + SO_4^{2-} \rightarrow HCO_3^- + HS^- + H_2O$ (e.g. Reeburgh, 1976). Methane is strongly depleted in ^{13}C relative to seawater DIC, therefore ^{13}C-depleted pore-water DIC indicates incorporation of light carbon from the anaerobic oxidation of methane (e.g. Haese et al., 2003). Characteristically, the maximum ^{13}C-depletion of DIC occurs within active zones of AOM (Ussler and Paull, 2008) which correspond with the SMT zones. As AOM increases pore-water DIC concentration and alkalinity, ^{13}C-depleted DIC is incorporated into authigenic carbonates which are used as a diagnostic indicator of past methane flux and AOM. Consequently, the $\delta^{13}C$ value of pore-water DIC is a critical parameter for understanding carbon cycling in methane-rich sediments and the possible origin of the methane.

* Corresponding author. Tel.: +86 20 85290315; fax: +86 20 85290315.
E-mail address: yfchen@gig.ac.cn (Y. Chen).

0009-2541/$ – see front matter © 2010 Elsevier B.V. All rights reserved.
doi:10.1016/j.chemgeo.2010.04.013

Hundreds of pockmarks are widespread on the seabed in Nyegga area (Bünz et al., 2003; Hjelstuen et al., 2010), which is located at the southern border of Vøring Plateau and 1–2 km away from the northern flank of the Storegga Slide — the world largest known exposed submarine landslide (Haflidason et al., 2004 and 2005). Pockmark G11 is ~200 m across and 12 m deep, and the most spectacular fluid flow feature at Nyegga (Hovland et al., 2005). A large accumulation of methane hydrates indicated by a prominent regional bottom simulating reflector (BSR) occurs in sediments in this region (e.g., Bünz et al., 2003 and 2004; Hustoft et al. 2007). The observed massive methane-derived authigenic carbonates and chemosynthetic communities (such as, tube worms and bacterial mats etc.) widespread on the seabed in Pockmark G11 suggested that the pockmark was caused by hydrocarbon flow in the past (e.g., Hovland et al., 2005; Mazzini et al., 2006; Hovland and Svensen, 2006). The occurrence of methane hydrate was indicated by the soupy structures in the cored sediments (Ivanov et al., 2007; 2010). It has been suggested that thermogenic methane from deep subsurface (Bünz et al. 2003 and 2004) or the mixed methane (e.g., Mazzini et al., 2006) might contribute to gas hydrate formation and shallow gas accumulations in Pockmark G11. Up to now, no detailed pore-fluid sampling has been conducted to study the characteristics of pore fluids in sediments from the pockmark.

Remotely operated vehicle (ROV) observations, and sampling of pore fluids and methane hydrates, were conducted by University of Bergen for the first time in Pockmark G11 in July–August 2008. Six sediment cores up to 3 m long were collected inside (5 cores) and outside (1 core) pockmark G11. The $\delta^{13}C$ values of DIC ($\delta^{13}C_{DIC}$), $\delta^{18}O$, and the chemical composition of pore fluids with respect to SO_4^{2-}, ΣH_2S, Cl^-, DIC, Ca^{2+}, and Mg^{2+} were determined to address (1) methane hydrate occurrence in sediments; (2) geochemical processes in methane-rich sediments and spatial methane fluxes; (3) the origin of methane; and (4) the potential sources of methane in Pockmark G11.

2. Geological setting

The Nyegga region is located at the southern border of the Vøring Basin, which is adjacent to the northern flank of the Storegga Slide (Fig. 1). The formation of this region was developed by several rifting phases in the Late Jurassic, the Late Cretaceous, and continental break-up between Scandinavia and Greenland in the late Paleocene–Early Eocene (Bjørnseth et al., 1997; Brekke, 2000). The Cenozoic sediments at Nyegga have been sub-divided into the Brygge, Kai and Naust Formations (Dalland et al., 1988). The youngest formation, i.e., the Late Plio-Pleistocene Naust Formation, is up to 1500 m thick, comprising glacigenic sediments deposited during the Northern Hemisphere Pleistocene glaciations (e.g. Hjelstuen et al., 1999). The underlying Miocene–early Pliocene Kai Formation is characterized by fine-grained hemipelagic siliceous oozes. The Kai Formation is heavily deformed due to polygonal faulting (Berndt et al., 2003). The basal sedimentary sequence is the Eocene–Oligocene Brygge Formation, mainly consisting of clay.

Pockmark G11 has been described by several authors (Hovland et al., 2005; Hovland and Svensen, 2006; Mazzini et al., 2006), and is found to be a complex pockmark among the numerous pockmarks and mounds observed at Nyegga area. It occurs at a water depth of ~750 m, and is ~200 m across and ~12 m deep. It was visited for ROV inspections and sampling of carbonates in 2003 and 2004 showing that living macro-benthos, chemosynthetic fauna such as tubeworms, and outcrops of authigenic carbonates were widespread on the seabed within Pockmark G11 (Hovland et al., 2005; Hovland and Svensen, 2006). The ROV-based, high resolution bathymetry of Pockmark G11 clearly demonstrates that G11 comprises a depression center surrounded by several high ridges most likely formed by authigenic carbonate ridges (Hovland and Svensen, 2006; Ivanov et al., 2010) (Fig. 2). A prominent, regional BSR occurs at ~280 mbsf below the pockmark (e.g., Bünz et al., 2003; Hustoft et al. 2007). Pockmark G11 is also connected to a subsurface chimney which originates from the base of inferred gas hydrate zone within Naust Formation (Hustoft et al., 2009).

3. Materials and methods

Sampling of pore fluids and methane hydrates in Pockmark G11 as well as seabed ROV observations were carried out during an expedition with R/V G.O.SARs in July–August 2008 in the Mid-Norwegian Sea. The ROV ARGUS is equipped with a high resolution video camera, two manipulators, one suction sample and three push cores.

3.1. Sampling

The sampling sites were chosen based on the high resolution TOPAS seismic profiles and the ROV seabed inspections. The bottom seawater temperatures in Pockmark G11 were measured by CTD (Conductivity–Temperature–Depth) during sampling.

Sediment samples were obtained by a gravity corer using 2–3 m long plastic liners. Four gravity cores (GS08-155-23GC, -25GC, -26GC and -41GC) were taken at different locations on the slopes of ridges inside Pockmark G11, one core GS08-155-22GC taken in the center of Pockmark G11, and one core GS08-155-28GC outside Pockmark G11 (Table 1, Fig. 2). The core recovery was 0.9–3.0 m, depending on location (Table 1).

The retrieved gravity cores were immediately cut into 1.2–1.5 m long sections and were split longitudinally into two halves on deck and marked as the working and archive halves. Because the air temperature was ~5 °C, all the sub-sampling was carried out on deck. The working halves were covered by plastic foil to avoid water loss due to evaporation and oxidation of pore-waters. Pore-waters were then sampled at 30–50 cm intervals based on visual lithologic variation, by Rhizon samplers. Up to 10 ml pore-water was collected within 3 h. Subsequently, pore-water was immediately preserved for various purposes (discussed below).

3.2. Methods

Aliquots of pore-water were preserved in glass vials for specific analyses and kept cool in a refrigerator onboard. They were shipped chilled with blue ice to different labs for shore-based measurements.

3.2.1. Concentrations of ions

Pore-water aliquots for dissolved pore-water constitutes including SO_4^{2-}, Cl^-, Ca^{2+} and Mg^{2+} were preserved in 2 ml glass vials and acidified with 0.1 ml supra-pure 65% HNO_3 to prevent H_2S oxidation from affecting pore-water sulfate concentrations (Joye et al., 2004) and carbonate precipitation (Wallmann et al., 2006). The sulfate and chloride concentrations were determined at the lab of Geological Survey of Norway (NGU), using a Dionex DX-120 ion chromatograph (IC). Pore-water samples were diluted 1:250 using deionized water so that sulfate and chloride could be simultaneously determined. Sulfate and chloride concentrations are expressed as millimolar units (mM). The analytical accuracy for both sulfate and chloride was ±2%, which was determined by measurement of the IAPSO (International Association for the Physical Sciences of the Oceans) standard seawater.

The concentrations of Ca^{2+} and Mg^{2+} were determined by an inductively coupled plasma optical emission spectrometer (ICP-OES) at the Dept. of Earth Science, University of Bergen. The analytical precision of IAPSO standard seawater is ±2%.

3.2.2. Sulfide concentrations

A 1-ml aliquot of interstitial water for the quantification of total dissolved hydrogen sulfide ($\Sigma H_2S = H_2S + HS^-$) concentration was transferred into a vial containing 0.5 ml of 20% zinc acetate solution. Sulfide was quantitatively preserved by precipitation as ZnS. Dissolved

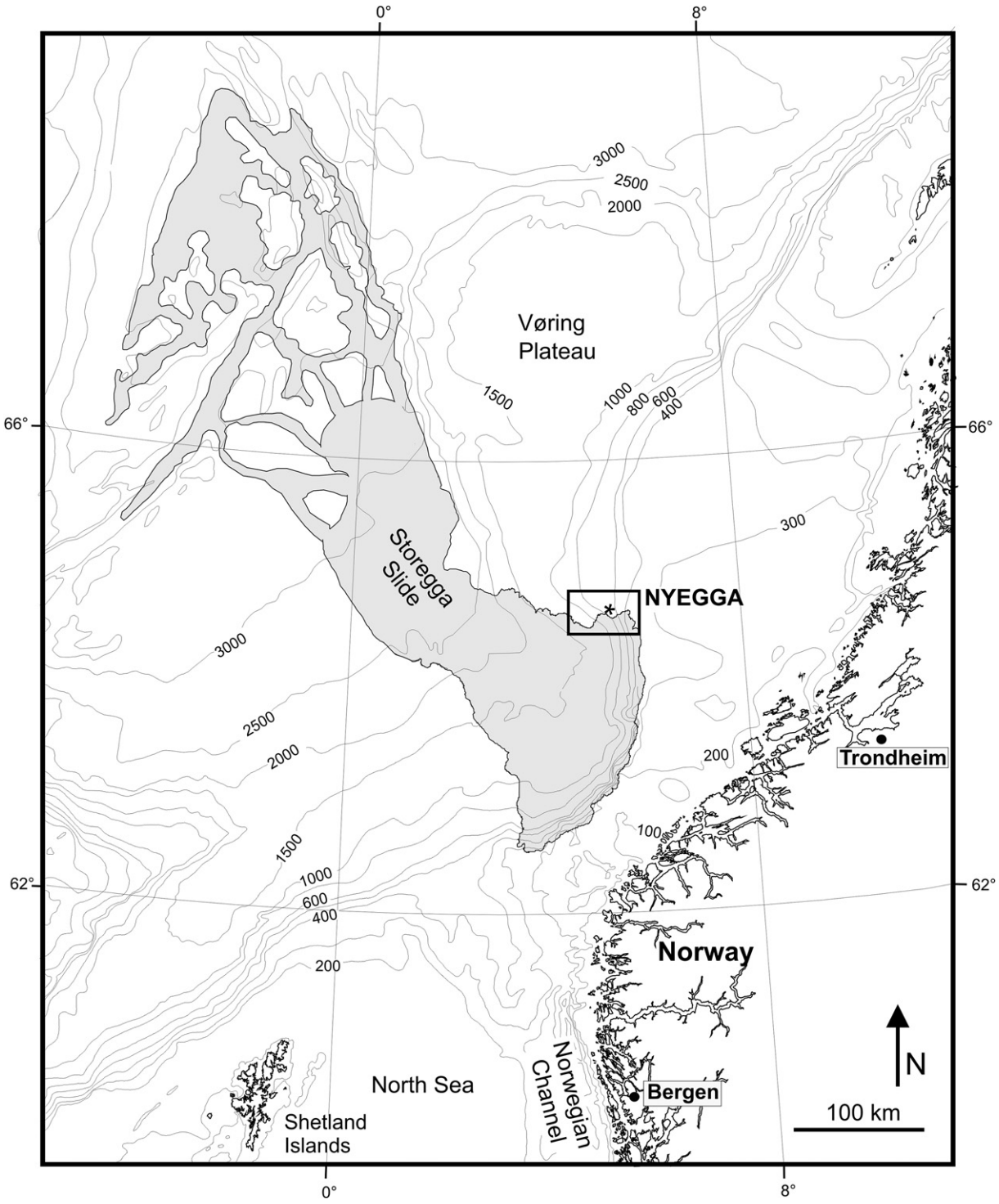

Fig. 1. Location map of Nyegga pockmark area on northern flank of the Storegga Slide of the mid-Norwegian continental margin. The position of pockmark G11 is indicated by a star.

sulfide was determined by the methylene blue method of Cline (1969) using a Thermo GENESYS 10 UV spectrophotometer with a Thermo spectrophotometric flow through a sample introduction system at the University of Bergen. Samples were diluted 2–300 times into a linear calibration curve range of 0–0.044 mM ΣH_2S before reagent addition. The detection limit of analysis is 0.001 mM.

3.2.3. DIC concentration and $\delta^{13}C$ values

About 2 ml pore-water for DIC ($=[CO_3^{2-}]+[HCO_3^-]+[CO_2]+[H_2CO_3]$) analyses was preserved with 10 µl saturated $HgCl_2$ solution in a vial without a headspace. The DIC concentration and $\delta^{13}C$ values were conducted at the stable isotope laboratory at Oregon State University, using continuous flow technology as described in Torres et al. (2005). The DIC concentrations and $\delta^{13}C$ values were determined using the same 0.3 ml water sample. The DIC concentration is expressed in mM and with precision of ±2%. The $\delta^{13}C_{DIC}$ is reported using standard δ notation (‰) with respect to the PDB standard, and with both precision and accuracy of ±0.15‰ (1σ).

3.2.4. Pore-water $\delta^{18}O$

Pore-water aliquots for $\delta^{18}O$ analysis were preserved in 4 ml glass vials without any chemical addition. Pore-water $\delta^{18}O$ values were

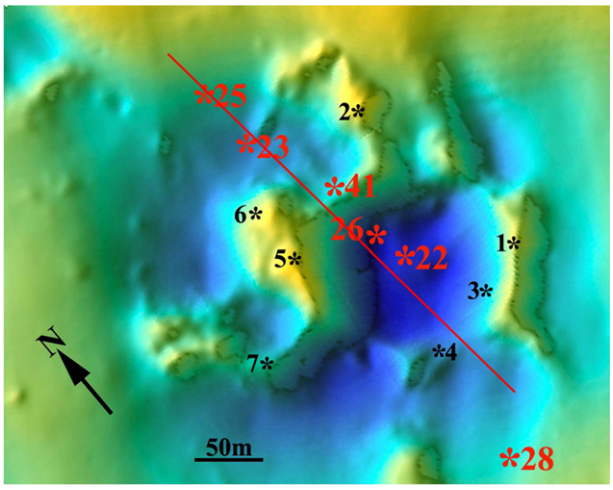

Fig. 2. The ROV-based bathymetry map of Pockmark G11and the coring positions. Numbers 22, 23, 25, 26, 28, 41indicated by red asterisks, represent for cores GS08-155-22GC, -23GC, -25GC, -26GC, -28GC, and -41GC. The red line represents the intended transect for sampling. The black numbered asterisks (1–7) indicate the locations of observed pingoes in 2004 by Hovland and Svensen (2006). The artificial illumination is from the NW.

determined at University of Kiel (Germany) using the H_2O–CO_2 equilibration method implemented using a continuous flow technology with helium carrier gas. The accuracy of the internal standards is ±0.1‰. The $\delta^{18}O$ of pore-water is reported using the standard δ notation (‰) with respect to Standard Mean Ocean Water (SMOW).

3.2.5. Sediment temperature and porosity

The temperature of sediments was measured at the lower end of each un-split section by digital thermometers. The sediment porosity was measured on the archive halves by multi Sensor Core Logger (MSCL) built by GEOTEK, at the Dept. of Earth Science, University of Bergen.

4. Results

4.1. Field observations

Seabed inspections with ROV show that the center of Pockmark G11 is flat. The seabed of the central depression consists of reddish brown clay with scattered shell rubbles (Fig. 3A), some macro-fauna assemblages of sponges, and possibly corals are surrounded by dense dead shell fragments (Fig. 3B). As observed by Hovland et al. (2005) and Hovland and Svensen (2006), the carbonate ridges are often enriched with clusters of macro-fauna, clusters of living pogonophora tubeworms and some patches of bacterial mats. In this study, massive patches of whitish bacterial mats (*Beggiatoa*) and living pogonophora tubeworms (D. Pornova, pers. comm.) were observed on the slope of a ridge (Fig. 3C), a large accumulation of dead *Isopordon* clams (Vesicomidae) (E. Krylova, pers. comm.) are scattered in between massive tubeworms and bacterial mats on the top of a ridge (Fig. 3D). *Isopordona* typically lives in chemically-reduced environments such as cold seeps. These dead bivalve patches were located away from massive bacterial mats and tubeworms (Fig. 3D). ROV push cores showed that the *pogonophora* tubeworms are slender with diameter of 1–2 mm and some tubeworms extended down to 5 cm below the seafloor (cmbsf). The *pogonophora* are regarded as an indicator species for cold seep environments because they harbor sulfide oxidizing symbionts (Carney, 1994). *Pogonophora* tubeworms and small patches of bacterial mats were found within the cracks of the carbonate pavements, which are covered with a thin sediment veneer (Fig. 3E). Bacterial mats (*Beggiatoa*) comprised filamentous sulfide-oxidizing bacteria and bright yellow granular elemental sulfur were observed (I.H. Steen, pers. comm.), indicating a sulfide enriched environment.

Although no visible gas/bubbles escaping to the water column were observed during the ROV video survey at Pockmark G11, ROV seabed observations and sampling of chemosynthetic fauna, bacterial mats and dead bivalve fragments, clearly demonstrate a typical cold seep environment has been persistent within Pockmark G11.

4.2. Cored sediment texture

The cored sediments comprise primarily soft, fine-grained, homogeneous green-grey hemi-pelagic clayey-silt, and with some intervals containing coarse drop-stones, overlain by a thin layer of brownish sediments. No obvious authigenic carbonate or bivalve fragments were observed in the cores. The core GS08-155-28GC was collected outside Pockmark G11 and black laminations occur throughout the core below 1.5 mbsf. The cores GS08-155-22GC, -23GC, -25GC, -26GC and -41GC were taken inside Pockmark G11. Core GS08-155-22GC contains soft and fine-grained sediments throughout the core, and no visual lithology or texture changes were observed. Moussey, gas expansion structures with gas voids (Paull and Ussler, 2001) were developed in core GS08-155-23GC (below 0.8 m), and -25GC (between 1.2–1.5 m, and below 1.8 m), and -26GC (below 0.7 m). These gas expansion structures are likely produced by high methane gas content. Core GS08-155-23GC is only 0.9 m long, characterized by bubble textures developing at the bottom of the core. Those are interpreted to be the result of gas expansion and gas hydrate dissociation during core recovery. Gas-hydrate layers are hard to penetrate with a gravity corer and most likely caused the short penetration.

For the first time, tabular methane hydrates (Fig. 4) were recovered in Pockmark G11. The methane hydrates occurred as thin, up to 0.5 cm thick horizontal and vertical plates in black mud from 0.75 mbsf to 1.0 mbsf (the end of core catcher), and these methane-hydrate plates extended across the full width of the core (Fig. 4).

4.3. Depth profiles of pore-water chloride and $\delta^{18}O$ values

Pore-water chloride concentrations ($n=45$) were analyzed for all the cores, whereas $\delta^{18}O$ values ($n=21$) were measured in

Table 1
Core locations, lengths and geochemical analyses.

Core number	Core length (m)	Latitude	Longitude	Analyses	Position
GS08-155-22GC	3.0	64° 39.812′N	05° 17.338′ E	SO_4^{2-}, Cl^-, DIC, $\delta^{13}C_{DIC}$, $\delta^{18}O$, Ca^{2+}, Mg^{2+}	Center
GS08-155-23GC	0.9	64° 39.833′N	05° 17.320′ E	SO_4^{2-}, Cl^-, DIC, $\delta^{13}C_{DIC}$, Ca^{2+}, Mg^{2+}	Depression
GS08-155-25GC	1.9	64° 39.850′N	05° 17.300′ E	SO_4^{2-}, Cl^-, DIC, $\delta^{13}C_{DIC}$, $\delta^{18}O$, Ca^{2+}, Mg^{2+}	Flank
GS08-155-26GC	1.9	64° 39.817′N	05° 17.308′ E	SO_4^{2-}, Cl^-, DIC, $\delta^{13}C_{DIC}$, Ca^{2+}, Mg^{2+}	Center slope
GS08-155-41GC	0.9	64° 39.824′N	05° 17.378′ E	SO_4^{2-}, Cl^-, $\delta^{18}O$	Ridge
GS08-155-28GC	3.0	64° 39.738′N	05° 17.329′ E	SO_4^{2-}, DIC, Cl^-, $\delta^{13}C_{DIC}$, Ca^{2+}, Mg^{2+},	Outside

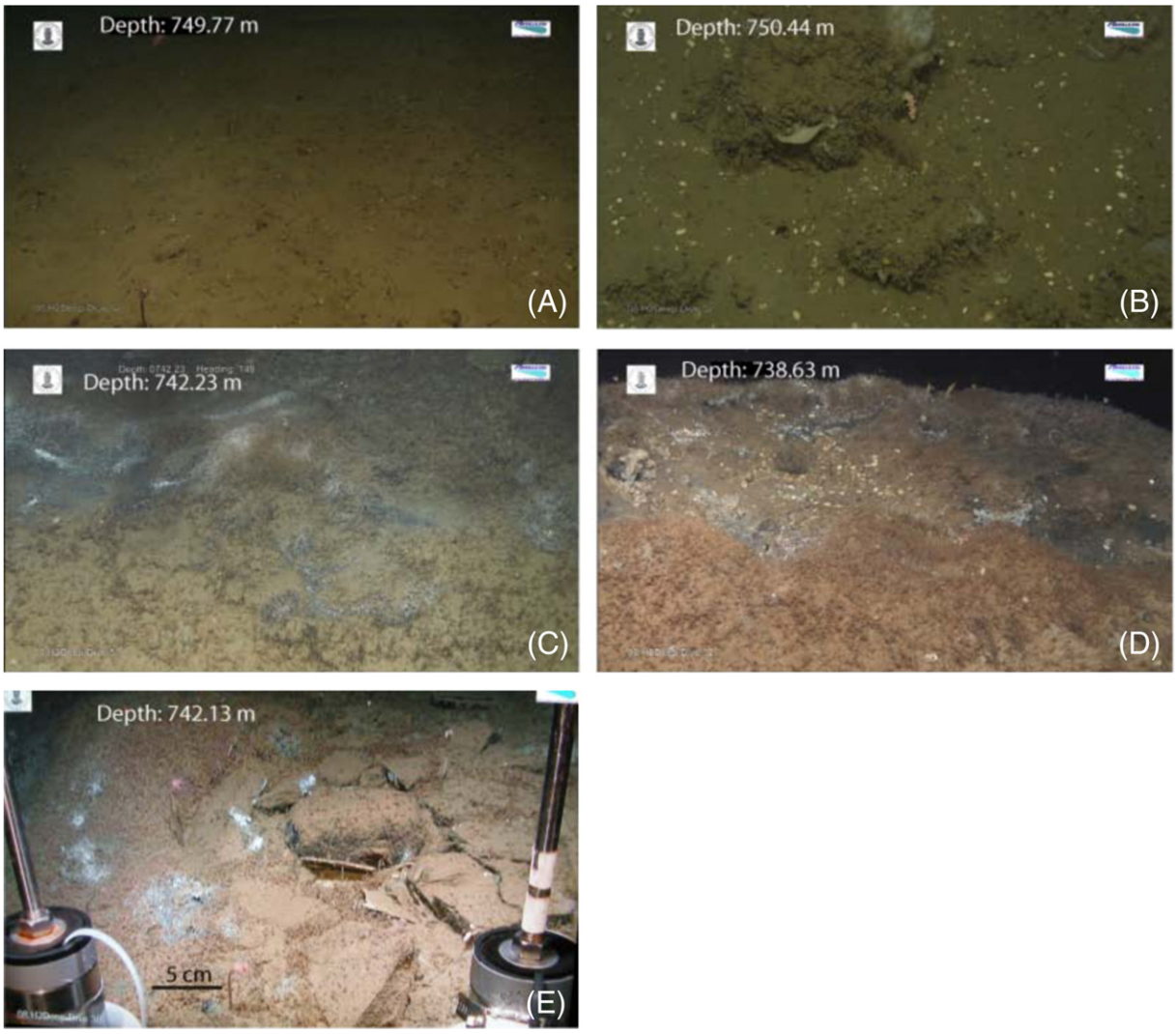

Fig. 3. ROV images of seabed in pockmark G11. (A) central depression of reddish brown seabed with scattered shell rubbles; (B) central depression with benthic fauna assemblage surrounded by dense patches of dead shell fragments; (C) massive patches of bacterial mats and tubeworm on the upper slope a ridge; (D) massive bacterial mats and tubeworms, and a large accumulation of dead *Isopordon* clams on the top of a ridge; (E) fractured carbonate pavements with small patches of bacterial mats within the cracks.

selected cores GS08-155-22GC, -25GC, and -41GC (Table 2). Chloride concentrations in cores GS08-155-22GC, -23GC, -25GC, -26GC and -28GC do not show any significant down-core trend, and vary between 525 and 561 mM (544 ± 9, $n = 29$). The chloride concentration of bottom water in Pockmark G11 area is calculated to be 545 mM according to the salinity data from CTD measurements. Therefore pore-water chloride concentrations in the 5 cores without methane hydrates are more or less the value of bottom seawater.

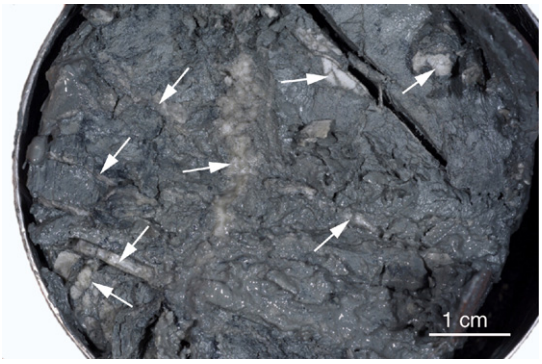

Fig. 4. Methane hydrates at the end of core GS08-155-41GC were recovered inside pockmark G11. Arrows are pointing to methane-hydrate slabs.

The $\delta^{18}O$ values of pore-water in selected cores GS08-155-22GC and -25GC were between 0.1 and 0.3‰ SMOW (0.2 ± 0.1, $n = 10$), which is consistent with the regional bottom water $\delta^{18}O$ value of 0.2 ‰ SMOW (Aagaard et al., 1989).

Pore-water Cl^- concentrations and $\delta^{18}O$ values show that no substantial amounts of gas hydrate occur in the sediments recovered in cores GS08-155-22GC, -23GC, -25GC, -26GC and -28GC. In contrast pore-water chloride concentrations and $\delta^{18}O$ values in GS08-155-41GC display a different pattern (Fig. 5). There is a large coupled change in Cl^- and $\delta^{18}O$ values when entering the gas-hydrate-bearing zone from 0.75 mbsf to the end of the core, with paired Cl^- decreases and $\delta^{18}O$ increases of 84.9 mM and 2.3‰ SMOW, 189.5 mM and 1.8‰ SMOW, 161.0 mM and 1.9‰ SMOW compared to the nearly constant values above 0.5 mbsf. Chloride and $\delta^{18}O$ values are negatively correlated as predicted for gas hydrate decomposition (Ussler and

Table 2
Geochemical data of cores GS08-155-22GC, 23GC, 25GC, 26GC and 28GC taken from Pockmark G11.

Core number	Depth (mbsf)	Cl^- (mM)	$\delta^{18}O$ (‰ SMOW)	SO_4^{2-} (mM)	H_2S (mM)	DIC (mM)	$\delta^{13}C_{DIC}$ (‰ PDB)	Ca (mM)	Mg (mM)
GS08-155-22GC	0.265	561.2	0.22	28.9		3.2	−10.4	10.6	55.7
GS08-155-22GC	0.58	560.8	0.19	28.1		3.6	−17.7	10.2	55.6
GS08-155-22GC	1	547.9	0.14	26.6		3.9	−19.3	10.1	54.7
GS08-155-22GC	1.29	541.8		26.3		3.8	−18.9	10.0	54.2
GS08-155-22GC	1.69	553.2		27.0		3.9	−17.8	10.0	54.2
GS08-155-22GC	2.03	548.9	0.19	26.4		3.9	−19.9	9.9	54.0
GS08-155-22GC	2.08	529.0		25.6				9.9	54.4
GS08-155-22GC	2.265	552.2	0.34	26.5				10.0	54.6
GS08-155-22GC	2.445	524.6		25.6		3.7	−19.3	10.0	54.3
GS08-155-22GC	2.81	540.6		26.3		3.7	−18.8	10.0	54.3
GS08-155-23GC	0.19	533.3		27.6	0.00	6.5	−28.7	7.2	53.7
GS08-155-23GC	0.48	539.0		5.9	5.04	21.3	−52.3	1.9	49.0
GS08-155-23GC	0.715	538.7		4.6	4.01	23.2	−51.0	1.4	47.8
GS08-155-23GC	0.8	536.0		5.0	1.44			1.0	46.6
GS08-155-23GC	0.86	526.0		4.7	1.69	23.1	−50.8	1.1	46.9
GS08-155-25GC	0.2	560.6	0.26	25.9	0.00	9.5	−39.5	6.8	56.8
GS08-155-25GC	0.43	554.1		5.0	5.16	21.5	−54.6	3.4	50.5
GS08-155-25GC	0.71	557.5	0.20	4.7	6.90	20.1	−52.8	3.4	59.6
GS08-155-25GC	1.075	550.2		4.3	4.66	19.9	−51.5	2.5	50.9
GS08-155-25GC	1.195	539.6	0.32	3.1	6.95	20.1	−50.1	2.6	50.9
GS08-155-25GC	1.335	537.4	0.30	3.2	6.99	20.6	−50.0	2.2	49.1
GS08-155-25GC	1.46	548.7		3.5	5.06	20.5	−49.1	2.2	49.6
GS08-155-25GC	1.61	550.3	0.17	3.2		19.4	−48.8	2.1	49.2
GS08-155-26GC	0.11	556.8		22.5		9.9	−45.7	8.0	55.3
GS08-155-26GC	0.42	547.2		4.6		19.4	−54.2	3.5	50.3
GS08-155-26GC	0.735	536.6		3.4		18.7	−49.5	2.8	49.5
GS08-155-26GC	1.08	555.3		3.9		18.7	−46.3	2.7	55.0
GS08-155-26GC	1.305	542.4		4.2		18.3	−44.0	1.9	47.7
GS08-155-26GC	1.715	535.5		4.3		18.3	−42.7	2.2	48.7
GS08-155-28GC	0.285	543.4	0.25	28.9	0.03	4.1	−14.6	10.0	54.8
GS08-155-28GC	0.84	565.7	0.24	28.0	0.03	5.2	−20.3	9.6	55.2
GS08-155-28GC	0.98	553.7		28.1	0.03	5.8	−23.4	9.0	54.1
GS08-155-28GC	1.3	562.9	0.25	27.5	0.03	6.2	−26.0	8.8	54.6
GS08-155-28GC	1.75	526.5		25.4	0.01	6.6	−27.2	8.4	52.9
GS08-155-28GC	1.99	531.7	0.18	25.7	0.02	6.7	−27.4	8.5	53.4
GS08-155-28GC	2.16	574.8	0.36	27.4	0.01	6.4	−27.4	8.7	54.6
GS08-155-28GC	2.28	576.8		27.1	0.02	6.6	−27.6	8.5	53.9
GS08-155-28GC	2.53	539.3		25.4	0.00		−30.3	8.7	54.5
GS08-155-28GC	2.78	554.5		26.1	0.00	7.1	−24.4	9.5	60.3
GS08-155-41GC	0.18	528.4	0.17	19.7				3.2	53.1
GS08-155-41GC	0.42	529.2	0.29	4.4				0.8	49.1
GS08-155-41GC	0.5	576.0	0.26	1.8				0.6	48.7
GS08-155-41GC	0.725			1.8					
GS08-155-41GC	0.8	84.9	2.34	2.0					
GS08-155-41GC	0.85	189.5	1.81	2.7				0.5	28.9
GS08-155-41GC	0.9	161.0	1.88	2.9					

DIC: dissolved inorganic carbon; blank: not measured due to not enough pore-water.

Paull, 2001). It is worthwhile to note that a higher Cl^- concentration of 576 mM occurs just above the methane hydrate layers.

4.4. Depth profiles of other pore-water constituents

Pore-water depth profiles of SO_4^{2-}, $\sum H_2S$, DIC, $\delta^{13}C_{DIC}$, Ca^{2+} and Mg^{2+} are shown in Fig. 6. In cores GS08-155-22GC and -28GC sulfate concentrations are nearly constant throughout the cores, and close to seawater values, ranging from 28.9 to 25.6 mM ($n=11$) and from 28.9 to 25.4 mM ($n=7$) respectively. DIC concentrations and $\delta^{13}C_{DIC}$ values occur in narrow ranges with DIC concentrations from 3.2 to 3.9 mM ($n=8$), and 4.1 to 7.1 mM ($n=9$); and $\delta^{13}C_{DIC}$ values from −10.4 to −19.9‰ PDB, and −14.6 to −30.3‰ PDB, respectively for -22GC and -28GC.

Sulfate concentrations decrease rapidly with depth from near seawater-like values to concentrations less than 5 mM below 0.4 mbsf in cores GS08-155-23GC, -25GC, -26GC, with a sharp break in slope at ~0.40–0.50 mbsf. Below 0.4 mbsf, the sulfate concentrations are relatively constant (3.2 to 5.0 mM) (Fig. 6). DIC concentrations increase with depth, with concentrations between 6.5–9.5 mM in the uppermost 0.20 m sediments, and increase sharply to maxima of 19.4–21.5 mM at ~0.40–0.50 mbsf, where the sulfate concentrations are at a minimum. DIC concentrations show little variation immediately below 0.40 mbsf to the bottom of the cores (up to 1.80 mbsf). The $\delta^{13}C_{DIC}$ values are distinctly depleted in ^{13}C, with values between −28.7 and −45.7‰ PDB in the uppermost 0.10–0.20 m sediments, and decrease sharply to minimal values of between −52.3 and −54.6‰ PDB at ~0.40–0.50 mbsf. Below ~0.40 mbsf, $\delta^{13}C_{DIC}$ shows a reversed trend and becomes ^{13}C-enriched with depth with values between −42.7 and −48.8‰ PDB at the end of the cores.

In cores GS08-155-23GC, -25GC, -26GC, calcium concentrations decrease sharply from below the value of normal seawater (~10.3 mM) in the uppermost 0.20 m sediments to minimum values of between 1.9 and 2.5 mM, at ~0.40–0.50 mbsf. Below 0.40 mbsf, the Ca^{2+} concentrations continue to decrease slowly with depth. Magnesium concentrations show the same down-core trend as the Ca^{2+}concentrations (Fig. 6).

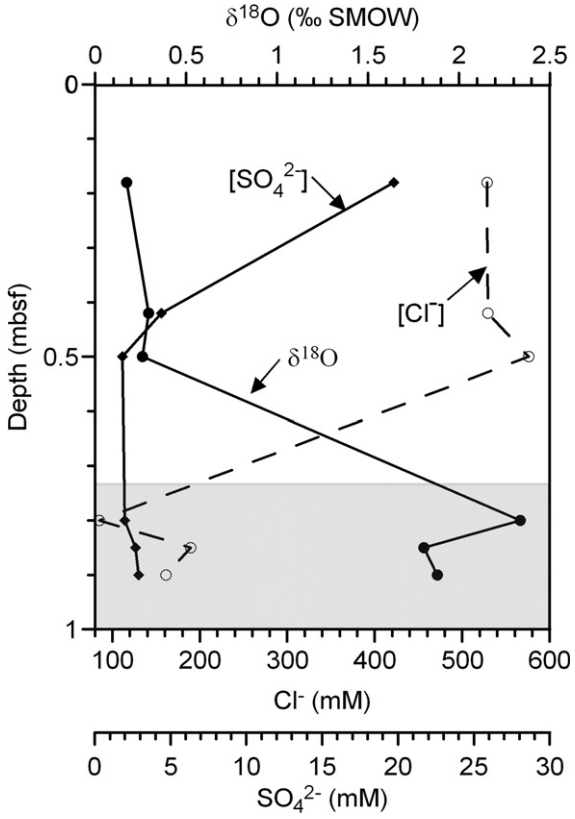

Fig. 5. The SO_4^{2-}, $Cl^-$and $\delta^{18}O$ depth profiles of core GS08-155-41GC, the shaded zone indicates where methane hydrate occurs.

5. Discussion

5.1. Methane hydrates in Pockmark G11

Horizontal and vertical methane-hydrate plates that spanned the full width of the core occurred from 0.75 mbsf to the bottom of the core GS08-155-41GC as shown in Fig. 4. This occurrence suggests that methane hydrates may exist deeper in the sediments elsewhere within Pockmark G11. More than 99.3% of the hydrate-bound gas is methane, and hydrate-bound methane is microbial, indicated by its $\delta^{13}C$ values (−72.4 to −66.2‰ PDB) and δD values (−202.0 to −198.0‰ SMOW) (Vaular et al., 2010). The coupled pore-water Cl^- concentration decrease and $\delta^{18}O$ increase below 0.75 mbsf (Fig. 5), clearly demonstrate the occurrence of disseminated and layers of methane hydrate in the sediments below 0.75 m. Methane hydrates exclude salt and incorporate ^{18}O-enriched water during formation, and release fresh water and ^{18}O-enriched water when hydrates dissociate (e.g., Ussler and Paull, 1995; Hesse, 2003). In Fig. 5, Cl^- concentration has a positive spike of 576 mM in the sediments just above the methane hydrate layers, which suggests that methane–hydrate formation is ongoing.

Pockmark G11 and upper 300 m sediments below it are well within the stability field of methane hydrate. The bottom water temperature of ~ −0.7 to −0.8 °C measured by CTD during this cruise, the water depth of ~750 m, and the regional geothermal gradient of 50–56 °C/km (Sundvor et al., 2000) indicate that the pressure and temperature conditions are appropriate for methane–hydrate formation within the upper 300 m sediments. This depth is consistent with the prominent BSR occurring at ~280 mbsf (e.g., Bünz et al., 2003; Bünz & Mienert, 2004; Hustoft et al., 2009). Methane hydrates recovered in the sediments below 0.75 m inside Pockmark G11 by this study suggest that methane hydrates may exist throughout the sediments overlying the BSR beneath Pockmark G11. More recent seismic studies by Hustoft et al (2009) showed that seismic reflectors bend upward toward the center of the chimney beneath Pockmark G11 above the BSR. The chimney structures are clearly not free-gas columns, because in that case they would be associated with velocity pull-downs. The formation of either gas hydrate or diagenetic carbonate along a fluid flow path would increase the seismic velocity (Paull et al., 2008) and create a velocity pull-up. However if the chimney was associated with authigenic carbonate, the carbonate will impede the methane fluxes upward migrating toward the seafloor, and then shallow SMT zones and methane hydrates would not be expected to occur near the seafloor as observed in this study. Thus methane hydrates probably occur at different depths above the BSR and are the likely cause of the velocity pull-ups within Pockmark G11.

5.2. Methane fluxes inferred from pore-water sulfate gradients

Pore-water sulfate diffusing downward from overlying seawater is the primary electron acceptors available for anaerobic oxidation of sedimentary organic matter and other reduced components such as methane. In anoxic marine sediments, pore-water sulfate is consumed by two microbially mediated sulfate reduction processes: (1) organoclastic sulfate reduction of organic matter, which is generally the most important degradation process for organic matter (OM) oxidation (e.g., Brener, 1980); and (2) anaerobic oxidation of methane (AOM) (Reeburgh, 1976), which is mediated by a syntrophic consortium of methanotrophic Archaea and sulfate-reducing bacteria (e.g., Boetius et al., 2000). As a consequence, AOM will create a sulfate–methane-transition (SMT) zone, where sulfate and methane are co-consumed. The net reactions are expressed stoichiometrically as following:

$$2CH_2O + SO_4^{2-} \rightarrow 2HCO_3^- + H_2S(\text{OMoxidation}) \quad (1)$$

$$CH_4 + SO_4^{2-} \rightarrow HCO_3^- + HS^- + H_2O(\text{AOM}) \quad (2)$$

The stoichiometry of the net Eqs. (1) and (2) shows that the ratios of the production of DIC to the consumption of sulfate differ between the two reactions: 2:1 for OM oxidation, and 1:1 for AOM (Masuzawa et al., 1992). A slope between 2 and 1 is a measure of the relative contribution of each sulfate-reduction pathway. Both sulfate reduction processes lead to elevated DIC concentrations in pore-waters, which in turn will lead to the precipitation of carbonate and cause a decrease of Ca^{2+} and Mg^{2+} concentrations. A plot of DIC produced corrected for Ca^{2+} and Mg^{2+} incorporation into authigenic carbonates [$(\Delta DIC + \Delta Ca^{2+} + \Delta Mg^{2+})$, computed relative to the typical seawater values of DIC (2.1 mM), Ca^{2+} (10.3 mM) and Mg^{2+} (53.2 mM) versus sulfate consumed [(ΔSO_4^{2-}), the difference between typical seawater sulfate concentration (28.9 mM) and the measured pore-water concentration], provides criteria for identifying the dominant oxidation processes causing reduction of pore-water sulfate concentration (Masuzawa et al., 1992). Because of bioturbation in the top 10–20 cm sediments, we ignored the data from these topmost layers. In cores GS08-155-22GC and -28GC, Mg^{2+} concentrations are a bit higher than typical seawater value. The reason will not be discussed here. Thus Mg^{2+} deficits are not included in these two cores.

Data from core GS08-155-28GC collected outside G11 plot on or near the slope of 2:1 (Fig. 7), clearly indicate that OM oxidation is the predominant sulfate reduction process. This suggests that, compared to cores inside pockmark G11, more labile organic carbon is available in sediments and that they have not been affected by nearby methane migration and pockmark formation. This is supported by the lamination textures developed in the core, suggesting the sediment column has been deposited normally, and has not been disturbed by

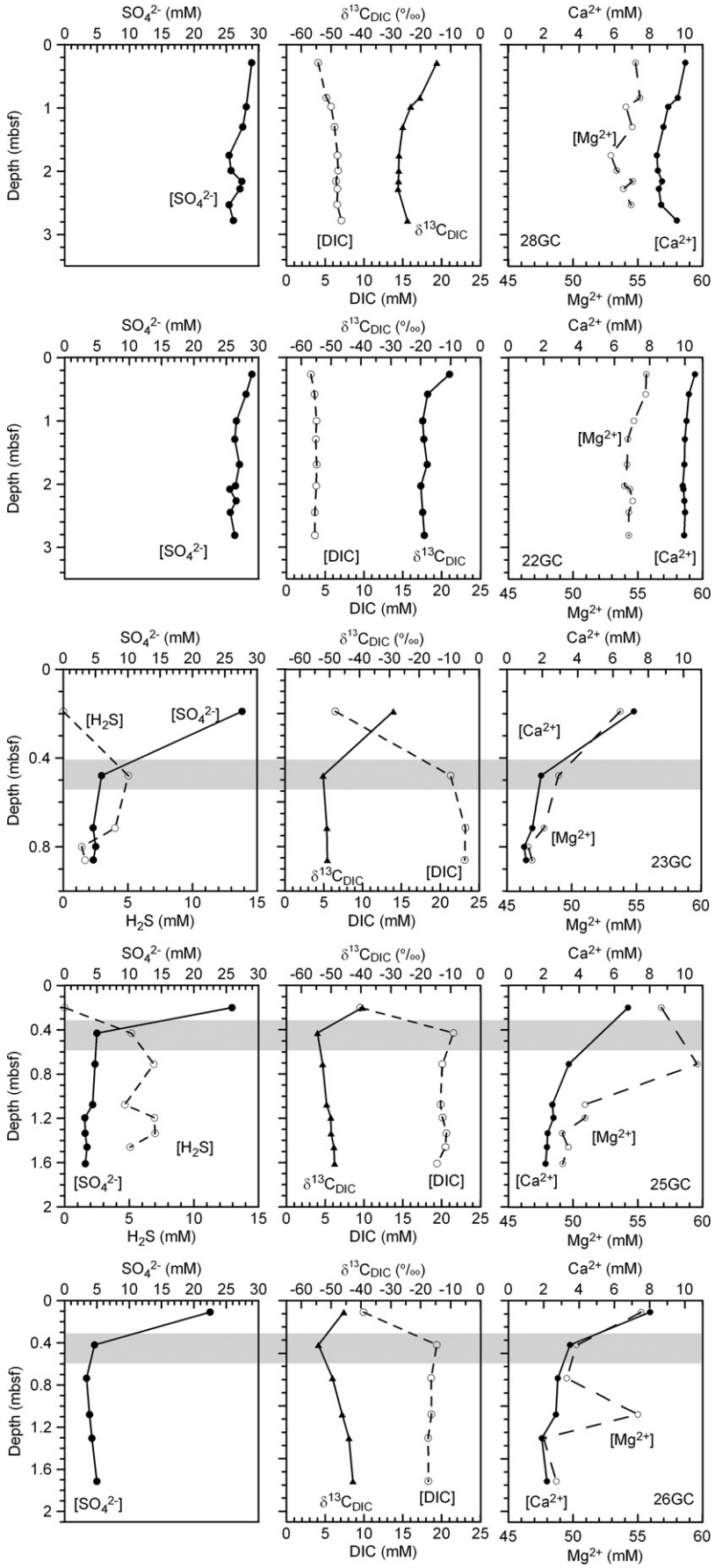

Fig. 6. Geochemical depth profiles shown for cores collected during this study. 22GC, 28GC, 23GC, 25GC and 26GC marked in the diagrams indicate cores GS08-155-22GC, -28GC, -23GC, -25GC and -26GC. Core 28GC was taken outside Pockmark G11, whereas the other cores were taken within the pockmark. The shaded zones indicate the SMT zones.

any gas or fluid expulsion. The pore-water $\delta^{13}C_{DIC}$ ranged from −30.3 to −14.6‰ PDB (mean = −24.9 ± 4.5‰ PDB, $n = 10$), clearly showing that DIC is mainly derived from *in situ* organic matter oxidation. This is because the $\delta^{13}C$ value of global marine organic matter is an average of −25‰ PDB (Anderson and Arthur, 1983).

Data from core GS08-155-22GC collected inside G11 cluster around the slope of 1:1 (Fig. 7), indicating that sulfate reduction by AOM is the dominant biogeochemical process. Throughout the cored 3 m long sediments, pore-water sulfate concentrations remain close to a seawater value (28.9 mM). Dead *Isopordon* clam fragments (Vesicomidae) (E. Krylova, pers. comm.) are found at a number of locations inside G11 (Fig. 3B), suggesting that AOM may have occurred in the past at depths shallower than 3 mbsf. A reduction in the upward migration of methane would have allowed sulfate from overlying seawater to subsequently diffuse into the sediments. This implies that upward flux of methane has decreased since *Isopordon* clams lived on the seafloor. The $\delta^{13}C_{DIC}$ values range from −10.4 to −19.9‰ PDB (mean = −17.8 ± 3.1‰ PDB, $n = 8$), indicating that no methane-derived carbon occurs presently in the DIC pool in the uppermost 3 m. Therefore, there is no methane seepage currently active in the center of Pockmark G11. This conclusion is supported by the observation that seafloor sediments are dark brown in color and no living chemosynthetic communities have been found in the central portion of Pockmark G11.

Data from the three other cores collected inside Pockmark G11 cluster between slopes of 2:1 and 1:1, with a slope of 1.4:1 for core GS08-155-23GC; and a slope of 1.2:1 fore cores GS08-155-25GC and -26GC (Fig. 7), suggesting that sulfate reduction in these cores is a mixture of OM oxidation and AOM. These ΔDIC to ΔSO_4^{2-} ratios are consistent with sulfate being reduced by electrons contributed from AOM (~60%), OM oxidation (~40%) in the core GS08-155-23GC, and AOM (~80%), and OM oxidation (~20%) in the cores GS08-155-25GC and -26GC. AOM is the dominant process for sulfate reduction below 0.4 mbsf in these three cores from the interior of G11. The highly ^{13}C-depleted DIC values (−45.7 to −54.6‰ PDB) (Fig. 6) support this observation.

It is important to note that sulfate concentrations are non-zero (from 3.2 to 5.0 mM) below the SMT in cores GS08-155-23GC, -25GC and -26GC. This is inconsistent with what is typically observed and predicted below the SMT. Luff and Wallman (2003) observed this phenomenon in Hydrate Ridge, and proposed that the non-zero sulfate values at and below SMT are due to hydrogen sulfide oxidation induced by penetration of oxygen into anoxic samples during pore-water sampling. However no negative correlation between sulfate and total hydrogen sulfide concentration at or below SMT is observed in the cores from inside G11 (Fig. 6) and there is no obvious oxidant (source of oxygen) in a quantity sufficient to produce the sulfate concentrations measured. Based on previous sampling experience, it is highly unlikely that exposure of the core samples to air can produce such large sulfate anomalies. Therefore, we believe that the non-zero sulfate concentrations are real but we have no plausible explanation for their occurrence.

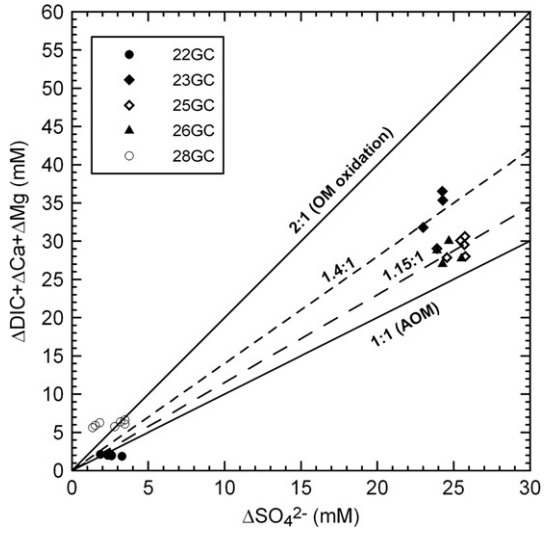

Fig. 7. Plot of sulfate consumed vs. DIC produced corrected for calcium and magnesium loss by authigenic carbonate precipitation. Diagonal lines indicate 1:1 and 2:1 ratios of DIC produced to sulfate consumed. Observed pore-water ratios are caused either by organic matter oxidation or AOM or a mixture of the two processes.

It is well-established that sulfate–methane-transition zone is characterized by maximum DIC concentrations and corresponding minimum $\delta^{13}C_{DIC}$ values within zones of *active* AOM (Ussler and Paull, 2008). The SMT zones in three cores from G11 are ~0.50 mbsf (GS08-155-23GC), and ~0.40 mbsf (GS08-155-25GC and -26GC), as shown in Fig. 6.

The depth of SMT is a particularly useful parameter to infer relative methane fluxes rates on a regional scale, and shallower SMT depths are caused by a higher methane flux (e.g., Borowski et al., 1996; Luff and Wallmann, 2003). The SMT depths at three coring sites inside Pockmark G11 (~0.40 to 0.50 mbsf) are much shallower than those (5 to 12 mbsf) observed ~10 km west of Pockmark G11 (Paull et al. 2007a and 2008). This suggests that the methane fluxes inside Pockmark G11 are much higher than other sites in Nyegga area, even though the fluid flow inside pockmark G11 appears to be spatially highly variable as indicated by the lack of a sulfate gradient in core GS08-155-22GC collected inside the pockmark.

Methane flux is difficult to quantify using pore-water methane concentrations measured on recovered cores. Based on limited measurements and modeling, *in situ* concentrations are much higher (~50 to 80 mM) relative to atmospheric saturation (~1.4 mM). Methane loss occurs during core recovery by exsolution and concentrations are typically ~1.4 mM when measured shipboard (Paull and Ussler, 2001). Because methane and sulfate are con-consumed at the SMT by AOM at a 1:1 stoichiometry and pore-water sulfate concentrations are not altered by pressure and temperature changes during sample recovery, the methane flux can be inferred using the sulfate concentration gradient above the SMT (e.g. Borowski et al., 1996). The sulfate diffusive flux can be calculated according to Fick's first law assuming steady state conditions (Brener, 1980):

$$J = -\Phi D_s \partial C / \partial x \tag{3}$$

where J is the diffusive flux (mmol m^{-2} yr^{-1}), Φ is the porosity (mean porosity above SMT zone), D_s is the sediment diffusion coefficient (cm^2 s^{-1}), C is the concentration of sulfate (mmol l^{-1}), and x is the sediment depth (m). The steepest concentration gradient into the SMT (Fig. 4) was used for calculations of the fluxes to get the best estimation. Sediment diffusion coefficients, *Ds*, of sulfate were calculated according to Boudreau (1997) from the measured porosities (Eq. 4):

$$D_s = D_0 / \left(1 - \ln\Phi^2\right) \tag{4}$$

The bottom sea water temperature is approaching to 0 °C. At 0 °C, seawater sulfate $D_0 = 5.0 * 10^{-6}$ cm^2 s^{-1} (Li and Gregory, 1974). The porosities of sediments are 0.64 (23GC), 0.68 (25GC) and 0.75 (26GC). Because upward migrating methane is almost entirely consumed, and AOM accounted for 60% (23GC) and 80% (25GC and 26GC) for the sulfate reduction as discussed previously in this section, the methane fluxes were estimated to be 60% and 80% of sulfate diffusive fluxes. The calculated methane fluxes are from 0.30 mol m^{-2} a^{-1} (23GC) to 0.44 mol m^{-2} a^{-1} (26GC) and 0.54 mol m^{-2} a^{-1} (25GC). Compared with those from worldwide methane hydrate areas, the methane fluxes in Pockmark G11 are much higher than those from Blake Ridge (0.02 mol m^{-2} a^{-1}) (Borowski, 2004), and Gulf of Mexico (0.02–

0.2 mol m^{-2} a^{-1}) (Coffin et al., 2008), but lower than those (8.7 to 51 mol m^{-2} a^{-1}) (Torres et al., 2002; Luff and Wallmann, 2003) over the southern summit of Cascadian Hydrate Ridge. Methane fluxes inside Pockmark G11 have been comparatively high although the upward methane flux appears to be diminishing near the center of the pockmark.

5.3. AOM and the origin of methane

Several lines of evidence indicate that AOM is ongoing today in the sediments in cores GS08-155-23GC, -25GC and -26GC (Fig. 6) inside Pockmark G11. 1) Extensive living chemosynthetic communities — *Beggiatoa* bacterial mats and pogonophora tube worms are widespread on the seafloor within G11, which indicates adequate amounts of hydrogen sulfide to support these organisms occur in the immediate subsurface. This implies active migration of methane-rich fluids toward the seafloor and production of hydrogen sulfide by AOM is occurring just beneath the seafloor; 2) the extremely ^{13}C depleted $\delta^{13}C_{DIC}$ values (−54.6 to −52.3‰) at the SMT and clearly indicate pore-water DIC is mainly derived from AOM rather than from other carbon sources; 3) ΔDIC corrected for calcium and magnesium deficits to ΔSO_4^{2-} ratios are consistent with AOM being the predominant process for sulfate reduction; and 4) headspace methane concentrations decrease from maximum values of 4.3 mM below the SMT to approaching 0 mM just above the SMT, indicating nearly complete methane consumption within the SMT (E.Vaular, pers. comm.).

It is well known there are two general mechanisms generating methane in marine sediments away from hydrothermal systems: microbial methane formed via CO_2-reduction or acetate fermentation, and thermogenic methane generated via organic matter maturation and/or thermal cracking. The stable carbon isotopic composition of methane offers a distinct proxy to differentiate these two methane sources: microbial methane having $\delta^{13}C$ values of typically more negative than −60‰, and thermogenic methane typically more positive than −50‰ (e.g. Whiticar, 1999).

Because $\delta^{13}C$ values of methane in the sediments/pore-waters are not available for G11, pore-water DIC and $\delta^{13}C_{DIC}$ values at the SMT are used to infer the origin and source of methane. Possible pore-water DIC sources at the SMT zone in marine sediments include mainly: 1) DIC diffusing from overlying seawater into the sediments or seawater DIC trapped within sediments during burial (*sw*); 2) DIC derived from degradation of sedimentary organic matter (*OM*); 3) DIC produced by AOM (*AOM*). At the SMT, the methane is nearly completely consumed; therefore DIC derived from AOM has the same carbon isotopic value as that of methane being oxidized.

A simple mass balance model can be used to discriminate sources of pore-water DIC (Borowski et al., 2000). In a closed system, the carbon isotopic composition of the carbon pool at the SMT can be expressed by:

$$\delta^{13}C_{DIC} = (X_{AOM})^*\left(\delta^{13}C_{methane}\right) + (X_{sw})^*\left(\delta^{13}C_{sw}\right) + (X_{OM})^*\left(\delta^{13}C_{OM}\right) \quad (5)$$

where X is the fraction of DIC contributed to the total DIC pool, $\delta^{13}C$ is the carbon isotopic composition, and the subscripts AOM, sw and OM refer to DIC donated from the sources listed above. The $\delta^{13}C_{sw}$ values are 0 ± 0.5‰ ($n=4$); pore-water $\delta^{13}C_{DIC}$ values are −52.3‰ (GS08-155-23GC), −54.6‰ (-25GC) and −54.2‰ (-26GC) at the SMT depths; the average global marine organic matter $\delta^{13}C = -25$‰ (Anderson and Arthur, 1983) is used for $\delta^{13}C_{om}$; the contribution fractions estimated from DIC and sulfate stoichiometries are 56% (AOM), 38% (OM) and 6% (sw) in core GS08-155-23GC, and 74% (AOM), 19% (OM) and 7% (sw) in cores both GS08-155-25GC and -26GC. The estimated $\delta^{13}C_{methane}$ values in uppermost 3 m sediments inside Pockmark G11 are −76.2‰ (-23GC), −65.3 ‰ (-25GC) and −66.8‰ (-26GC), definitely demonstrating methane involved in AOM in these 3 cores is microbial in origin.

One previously obtained interstitial methane sample collected from Pockmark G11 has a $\delta^{13}C$ value of −69.3‰ PDB (Hovland et al., 2005). Hydrate-bound methane from two cores including core -41GC inside Pockmark G11 has $\delta^{13}C$ values ranging between −66.2 and −72.4‰ PDB (with a mean of −69.0 ± 1.9 ‰, $n=14$) (Vaular et al., 2010). Measured methane $\delta^{13}C$ values are nearly the same as the estimated $\delta^{13}C$ values of methane involved in AOM in shallow sediments in cores GS08-155-23GC, -25GC and -26GC. In addition, the δD values of hydrate-bound methane are between −201 and −202‰ SMOW (−201.5 ± 0.6 ‰, $n=4$) (Vaular et al., 2010), which is consistent with the methane in Pockmark G11 being generated by microbial CO_2 reduction. Model calculations and limited isotopic data suggest that methane in pockmark G11 is microbial in origin and may be derived from a common methane pool.

5.4. Potential sources of microbial methane

Microbial methane in shallow sediments and hydrates inside Pockmark G11 may have resulted from *in situ* or local methanogenesis, from fossil hydrate recycling, or from fluid advection from deep strata associated with the polygonal fault systems in the Kai Formation (Berndt et al., 2003; Bünz and Mienert, 2004).

In cores -23GC, -25GC and -26GC, pore-water DIC affected by AOM have $\delta^{13}C_{DIC}$ values that gradually become less ^{13}C-depleted with depth below the SMT: −52.3 to −50.8‰ (0.4–0.9 mbsf in -23GC), −54.6 to −48.8‰ (0.4–1.6 mbsf in -25GC) and −54.2 to −42.7‰ (0.4–1.72 mbsf in -26GC). This reversal in $\delta^{13}C_{DIC}$ below the SMT might be explained by the onset of methane generation. During methanogenesis, ^{13}C-depleted DIC in pore-water is preferentially reduced to methane via:

$$4H_2 + CO_2 \rightarrow CH_4 + 2H_2O$$

which causes the residual DIC pool to become ^{13}C-enriched. However measured sulfate concentrations below SMT are from 3.2 to 5.0 mM, (4.1 ± 0.7 mM, $n=13$), which are thought to inhibit *in situ* methane generation. This is due to sulfate reducers outcompeting methanogens for substrate such as H_2 and acetate (e.g., Reeburg, 2007). Meanwhile DIC concentrations are nearly constant below the SMT (20.2 ± 1.5 mM, $n=15$, suggesting that there is limited or no *in situ* methanogenesis. Bünz et al. (2003) suggested that the low total organic carbon contents of ~0.5 wt.% in the upper ~400 m Naust Formation sediments are not sufficient to produce enough methane for the methane system in pockmark G11 area. This is consistent with present thermal structure of the upper 1 km of the sediment column (present-day bottom water temperature of ~0°C and a regional geothermal gradient of 50 °C/km) because microbial methane generation occurs at low temperatures (<50 °C) (e.g., Claypool and Kvenvolden, 1983; Reeburg, 2007), This depth is approximately the base of the Naust Formation. Although there is limited or no *in situ* or local methanogenesis in Pockmark G11, and little potential for production of methane in the sediments in the underlying Naust Formation, methane may have migrated from a deeper geologic source.

The Kai Formation occurs below 1.5 km where the geothermal gradient predicts that sediment temperatures will exceed 75 °C, conditions favourable for thermogenic methane generation. However, based on measured methane $\delta^{13}C$ values and δD values from Vaular et al. (2010) and modelled $\delta^{13}C$ values, the methane that occurs in the shallow sediments and methane hydrates is microbial in origin. As a consequence, deeply-sourced methane-rich fluids transported upward along the polygonal faults in Kai Formation can be excluded.

Thus, an alternative mechanism for methane accumulation and migration needs to be identified.

Several lines of evidence show that microbial methane could be derived from recycling of fossil methane hydrates. First, the occurrence of methane hydrate indicated by BSRs implies that there is a large quantity of methane carbon in the sediment system. Secondly, the widespread methane-derived authigenic carbonates in Pockmark G11 area are depleted in ^{13}C ($\delta^{13}C = -49.4$ to -52.1‰ PDB) but enriched in ^{18}O ($\delta^{18}O = 5.2$ to 6.4‰PDB), indicating authigenic carbonates outcroping on the present seafloor are linked to the fossil methane hydrate dissociation events (Mazzini et al., 2006). Measured $^{87}Sr/^{86}Sr$ ratios (0.709168 ± 0.000018) of the authigenic carbonates (Mazzini et al., 2006) are close to the seawater value of the late Pleistocene, indicating that methane hydrate decomposition might have occurred in the late Pleistocene.

The methane fluxes resulting from hydrates breakdown must be episodic and not continuous eruption, because the authigenic carbonates which form initially in the subsurface in association with the SMT (Paull et al., 2007b; Chen et al., 2007) crop out on the seafloor today and are highly fractured. Tubeworms and bacterial mats were observed in between carbonate fractures (Fig. 3E). Pockmark G11 appears to have been caused by the episodic leakage of methane-enriched fluids derived from local sources.

6. Summary and conclusions

Spatial differences in geochemical profiles and seabed inspections suggest high spatial heterogeneity in the upward flux of methane-rich fluids within and surrounding pockmark G11. In active methane upward-migrating sites, methane fluxes calculated from pore-water sulfate concentration profiles are between 0.30 and 0.54 mol m^{-2} a^{-1}. Upward-migrating methane inside pockmark G11 has been completely oxidized at the SMT from ~0.40 to 0.50 mbsf by downward-diffusing sulfate from overlying seawater. The $\delta^{13}C$ of methane estimated from measured DIC concentrations and $\delta^{13}C_{DIC}$ using a simple mass balance modeling ranges from -65.3 to -76.2‰ PDB, suggesting that methane in the shallow sediments inside Pockmark G11 is microbial in origin. This is consistent with the conclusion that hydrate-bound methane in G11 is formed by microbially-mediated CO_2-reduction (Vaular et al., 2010). For the first time, tabular methane hydrate samples were recovered in the uppermost 1 m sediments inside Pockmark G11, suggesting that methane hydrates may occur beneath the pockmark down to the BSR (~280 mbsf). Pore-water geochemical data and seabed observations suggest that Pockmark G11 was formed by several methane-rich fluid expulsions. Episodic upward methane fluxes are derived from the recycling of methane hydrates during sediment burial. All these lines of evidence lead us to propose that the ridges inside pockmark G11 were active with methane fluxes not only in the past but are also currently active, and that the carbonate pavements have been exhumed and fractured by recent fluid expulsion.

Acknowledgements

We are grateful to Walter S. Borowski for his constructive suggestions and fruitful comments for the review of the manuscript. We thank Associate Prof. I. Thorseth (University of Bergen) for kind help on geochemical analyses in geochemical lab at the Dept. of Earth Science, and B. Kjøsnes (NGU) for ion analyses. Discussion with Prof. V. Melezhik (NGU) and Dr. Dr. X.P. Hu (University of Georgia) is appreciated. We also thank Statoil for detailed bathymetric data. This study was made possible by the program GANS ("Gas hydrates on the Norway-Barents Sea-Svalbard margin", Contract No. 175969/S30), and was partially supported by the NSF of China (Grants: 40725011 and U0733003).

References

Aagaard, P., Egeberg, P.K., Smalley, P.C., 1989. Diagenetic reactions in Leg 104 sediments inferred from isotope and major element chemistry of interstitial waters. In: Eldholm, O., Thiede, J., Taylor, E. (Eds.), Proc. ODP, Sci. Results, 104. Texas A&M University, College Station, TX, pp. 273–280.

Anderson, T.F. and Arthur, M.A., 1983. Stable Isotopes of oxygen and carbon and their application to sedimentologic and paleoenvironmental problems. In: Arthur, M.A., Anderson, T.F., Kaplan, I.R. and Veizer, J. (*Eds.*) *Stable Isotopes in Sedimentary Geology, SEPM Short Course, No. 10:* 1-1-1-151.

Berndt, C., Bünz, S., Mienert, J., 2003. Polygonal fault systems on the Mid-Norwegian margin: a long-term source for fluid flow. In: Rensbergen, P.V., Hillis, R., Maltman, A., Morley, C. (Eds.), Subsurface Sediment Mobilization: Geol. Soc. Lond. Spec. Publ., 216, pp. 283–290.

Brekke, H., 2000. The tectonic evolution of the Norwegian Sea continental margin, with emphasis on the Vøring and Møre basins. In: Nøttvedt, A. et al. (Eds.), Dynamics of the Norwegian Margin. Geological Society of London Special. Publication 167, 327–378.

Bjørnseth, H.M., Grant, S.M., Hansen, E.K., Hossack, J.R., Robert, D.G., Thompsom, M., 1997. Structural evolution of the Voring Basin, Norway, during the Late Cretaceous and Palaeogene. J.Geol. Soc. 154, 559–563.

Boetius, A., Ravenschlag, K., Schubert, C.J., Rickert, D., Widdel, F., Gieseke, A., Amann, R., Jørgensen, B.B., Witte, U., Pfannkuche, O., 2000. A marine microbial consortium apparently mediating anaerobic oxidation of methane. Nature 407 (6804), 623–626.

Borowski, W.S., 2004. A review of methane and gas hydrates in the dynamic, stratified system of the Blake Ridge region, offshore southeastern North America. Chem. Geol. 205, 311–346.

Borowski, W.S., Hoehler, T.M., Alperin, M.J., Rodriguez, N.M., Paull, C.K., 2000. Significance of anaerobic methane oxidation in methane-rich sediments overlying the Blake Ridge and Carolina Rise. Proc. ODP Sci. Results 164, 87–99.

Borowski, W.S., Paull, C.K., Ussler III, W., 1996. Marine pore-water sulfate profiles indicate in situ methane flux from underlying gas hydrate. Geology 24 (7), 655–658.

Boudreau, B.P., 1997. Diagenetic models and their implementation. Springer-Verlag.

Brener, R.A., 1980. Early Diagenesis—A Theroretical Approach. Princeton University Press.

Bünz, S., Mienert, J., 2004. Acoustic imaging of gas hydrate and free gas at the Storegga Slide. J. Geophys. Res. 109, B04102. doi:10.1029/2003JB002863.

Bünz, S., Mienert, J., Berndt, C., 2003. Geological controls on the Storegga gas-hydrate system of the mid-Norwagian continental margin. Earth Planet. Sci. Lett. 209, 291–307.

Carney, R.S., 1994. Consideration of the oasis analogy for chemosynthetic communities at Gulf of Mexico hydrocarbon vents. Geo-Mar. Lett. 14, 149–159.

Chen, Y., Matsumoto, R., Paull, C.K., Ussler, W.I.I.I., Lorenson, T., Hart, P., Winters, W., 2007. Methane-derived authigenic carbonates from the northern Gulf of Mexico—MD02 Cruise. J. Geochemical Explor. 95, 1–15.

Claypool, G.E., Kvenvolden, K.A., 1983. Methane and other hydrocarbon gases in marine sediment. Ann. Rev. Earth Planet. Sci. 11, 299–327.

Cline, J.D., 1969. Spectrophotometric determination of hydrogen sulfide in natural waters. Limnol. Oceanogr. 14, 454–458.

Coffin, R., Hamdan, L., Plummer, R., Smith, J., Gardner, J., Hagen, R., Wood, W., 2008. Analysis of methane and sulfate flux in methane-charged sediments from the Mississippi Canyon, Gulf of Mexico. Mar. Petrol. Geol. 25, 977–987.

Dalland, A., Augedahl, H.O., Komstad, K., Ofstad, K., 1988. The post-Triassic succession of the mid-Norwegian shelf. In: Dalland, A., Worsley, D., Ofstad, K. (Eds.), A lithostratigraphic scheme for the Mesozoic and Cenozoic succession offhshore Mid- and northern Norway. Norwegian Petroleum Directorate Bulletin, No.4, pp. 5–42.

Dickens, G.R., 1999. The blast in the past. Nature 401 (6755), 752–755.

Haese, R.R., Meile, C., Van Cappellen, P., De Lange, G.J., 2003. Carbon geochemistry of cold seeps: methane fluxes and transformation in sediments from Kazan mud volcano, eastern Mediterranean Sea. Earth Planet. Sci. Lett. 212, 361–375.

Haflidason, H., Sejrup, H.P., Nygård, A., Mienert, J., Bryn, P., Lien, R., Forsberg, C.F., Berg, K., Masson, D., 2004. The Storegga Slide: architecture, geometry and slide-development. Mar. Geol. 213, 201–234.

Haflidason, H., Lien, R., Sejrup, P., Forsberg, C.F., Bryn, P., 2005. The dating and morphometry of the Storegga Slide. Mar. Petrol. Geol. 22, 123–136.

Hesse, R., 2003. Pore-water anomalies of submarine gas-hdyrate zones as tool to assess hydrate abundance and distribution in the subsurface. What have we learned in the past decade? Earth-Sci. Rev. 61, 149–179.

Hjelstuen, B.O., Eldholm, O., Skogeseid, J., 1999. Cenozoic evolution of the northern Vøring margin. Geol. Soc. Am. Bull. 111 (12), 1792–1807.

Hjelstuen, B.O., Haflidason, H., Sejrup, H.P. and Nygård, A., 2010. Sedimentary and structural control on pockmark development—evidence from the Nyegga pockmark field, NW European margin. Geo-Marine Letters 30, 221–230.

Hovland, M., Judd, A.G., 1988. Seabed pockmarks and seepages: impact on geology, biology and marine environment. Graham and Trotman, London. 565 pp.

Hovland, M., Svensen, H., 2006. Submarine pingoes: indicators of shallow gas hydrates in a pockmark at Nyegga, Norwegian Sea. Mar. Geol. 228, 15–23.

Hovland, M., Svensen, H., Forsberg, C.F., Johansen, H., Fichler, C., Fosså, J.H., Jonsson, R. And, Rueslåtten, H., 2005. Complex pockmarks with carbonate-ridges off mid-Norway: products of sediment degassing. Mar. Geol. 218, 191–206.

Hustoft, S., Mienert, J., Bünz, S., Nouzé, H., 2007. High-resolution 3D-seismic data indicate focused fluid migration pathways above polygonal fault systems of the mid-Norwegian margin. Mar. Geol. 245, 89–106.

Hustoft, S., Dugan, B., Mienert, J., 2009. Effects of rapid sedimentation on developing the Nyegga pockmark field: constraints from hydrological modeling and 3-D seismic data, offshore mid-Norway. Geochem. Geophys. Geosystems 10, Q06012. doi:10.1029/2009GC002409.

Gay, A., Lopez, M., Ondreas, H., Charlou, J.L., Sermondadaz, G., Cochonat, P., 2006. Seafloor facies related to upward methane flux within a Giant Pockmark of the Lower Congo Basin. Mar. Geol. 226, 81–95.

Ivanov, M., Mazzini, A., Blinova, V., Kozlova, E., Laberg, J-S., Matreeva, T., Taviani, M. and Kaskov, N., 2010. Seep mounds on the southern Vøring Plateau (offshore Norway). Marine and Petroleum Geology 27 (6), 1235–1261.

Ivanov, M., Westbrook, G.K., Blinova, V., Kozlova, E., Mazzini, A., Houzé, H., Minshull, T.A., 2007. First sampling of gas hydrate from the Vøring Plateau. EOS 88 (19), 209–216.

Joye, S.B., Boetius, A., Orcutt, B.N., Montoya, J.P., Schulz, H.N., Erickson, M.J., Lugo, S.K., 2004. The anaerobic oxidation of methane and sulfate reduction in sediments from Gulf of Mexico cold seeps. Chem. Geol. 205 (3/4), 219–238.

Kvenvolden, K.A., 1993. Gas hydrates — geological perspective on global change. Rev. Geophys. 31, 171–183.

Li, Y.-H., Gregory, S., 1974. Diffusion of ions in sea water and in deep-sea sediments. Geochim. Cosmochim. Acta 38, 703–714.

Luff, R., Wallmann, K., 2003. Fluid flow, methane fluxes, carbonate precipitation and biogeochemical turnover in gas hydrate-bearing sediments at Hydrate Ridge, Cascadia Margin: numerical modeling and mass balances. Geochim. Cosmochim. Acta 67 (18), 3403–3421.

Masuzawa, T., Handa, N., Kitagawa, H., Kusakabe, M., 1992. Sulfate reduction usign methane in sediments beneath a bathyal 'cold seep' giant clam community off Hatsumshima Island, Sagami Bay, Japan. Earth Planet. Sci. Lett. 110, 39–50.

Mazzini, A., Svensen, H., Hovland, M., Planke, S., 2006. Comparison and implications from strikingly different authigenic carbonates in a Nyegga complex pockmarkG11, Norwegian Sea. Mar. Geol. 231, 89–102.

Paull, C.K., Ussler III, W., Maher, N., Greene, H.G., Rehder, G., Lorenson, T., Lee, H., 2002. Pockmarks off Big Sur, California. Mar. Geol. 181, 323–335.

Paull, C.K., Ussler III, W., Holbrook, W.S., 2007a. Assessing methane release from the colossal Storegga submarine landslide. Geophys. Res. Lett. 34. doi:10.1029/2006GL028331.

Paull, C.K., Ussler, III, W., Peltzer, E., Brewer, P., Keaten, R., Mitts, P., Nealon, J., Greinert, J., Herguera, J.-C., Perez, E., 2007b. Authigenic carbon entomed in methane-soaked sediments from the northeastern transform margin of the Guaymas Basin: Gulf of California, Deep Sea Research II., vol., 54, pp. 1240–1267.

Paull, C.K., Ussler III, W., Holbrook, W.S., Hill, T.M., Keaten, R., Mienert, J., Haflidason, H., Johnson, J.E., Winters, W.J., Lorenson, T.D., 2008. Origin of pockmarks and chimney structures on the flanks of the Storegga Slide, offshore Norway. Geo-Mar. Lett. 28, 43–51.

Paull, C.K., Ussler III, W., 2001. History and significance of gas sampling during DSDP and ODP drilling associated with gas hydrates. In: Paull, C.K., Dillon, W.P. (Eds.), Natural Gas Hydrates: Occurrence, Distribution, and Detection: AGU Geophysical Monograph, 124, pp. 53–66.

Reeburgh, W.S., 1976. Methane consumption in Cariaco Trench waters and sediments. Earth Planet. Sci. Lett. 28, 337–344.

Reeburg, W.S., 2007. Oceanic methane biogeochemistry. Chem. Rev. 107, 486–513.

Sundvor, E., Eldholm, O., Gladczenko, T.P., Planke, S., 2000. Norwegian-Greenland Sea thermal field. In: Nøttvedt, A. (Ed.), Dynamics of the Norwegian Margin. Geological Society of London, Special Publication, pp. 397–410.

Torres, M.E., McManus, J., Hammond, D.E., de Angelis, M.A., Hesschen, K.U., Colbert, S.L., Tryon, M.D., Brown, K.M., Suess, E., 2002. Fluid and chemical fluxes in and out of sediments hosting methane hydrate deposits on Hydrate Ridge, OR, I: Hydrological provinces. Earth Planet. Sci. Lett. 201, 525–540.

Torres, M.E., Mix, A.C., Rugh, W.D., 2005. Precise $\delta^{13}C$ analysis of dissolved inorganic carbon in natural waters using automated headspace sampling and continuous flow mass spectrometry. Limnol. Oceanogr. Methods 3, 349–360.

Ussler III, W., Paull, C.K., 2008. Rates of anaerobic oxidation of methane and authigenic carbonate mineralization in methane-rich deep-sea sediments inferred from models and geochemical profiles. Earth Planet. Sci. Lett. 266, 271–287.

Ussler III, W., Paull, C.K., Boucher, J., Friederich, G.E., Thomas, D.J., 2003. Submarine pockmarks: a case study from Belfast Bay, Maine. Mar. Geol. 202, 175–192.

Ussler III, W., Paull, C.K., 1995. Effects of ion exclusion and isotopic fractionation on pore water geochemistry during gas hydrate formation and decomposition. Geo-Mar. Lett. 15, 37–44.

Vaular, E., Barth, T., Haflidason, H., 2010. The geochemical characteristics fo the hydrate-bound gases from the Nyegga pockmark field, Norwegian Sea. Org. Geochem. 41, 437–444.

Wallmann, K., Aloisi, G., Haeckel, M., Obzhirov, A., Pavlova, G., Tishchenko, P., 2006. Kinetics of organic matter degradation, microbial methane generation, and gas hydrate formation in anoxic marine sediments. Geochim. Cosmochim. Acta 70, 3905–3927.

Whiticar, M.J., 1999. Carbon and hydrogen isotope systematic of bacterial formation and oxidation of methane. Chem. Geol. 161 (1–3), 291–314.